

Quantum Circuit Transformation Based on Subgraph Isomorphism and Tabu Search^{*}

First Aaaaaauthor¹[0000-*ereer*1111-2222-3333], Second Author^{2,3}[1111-2222-3333-4444], and Third Author³[2222--3333-4444-5555]

¹ Princeton University, Princeton NJ 08544, USA

² Springer Heidelberg, Tiergartenstr. 17, 69121 Heidelberg, Germany

lncs@springer.com

<http://www.springer.com/gp/computer-science/lncs>

³ ABC Institute, Rupert-Karls-University Heidelberg, Heidelberg, Germany
{abc,lncs}@uni-heidelberg.de

Abstract. The goal of quantum circuit transformation is to construct mappings from logical quantum circuits to physical ones in an acceptable amount of time, and in the meantime to introduce as few auxiliary gates as possible. We present an effective approach to constructing the mappings. It consists of two keys steps: one makes use of a combined subgraph isomorphism (CSI) to initialize a mapping, the other dynamically adjusts the mapping by using a Tabu Search based transformation (TST). Our experiments show that, compared with the VF2 algorithm recently considered in the literature, CSI can save 22.26% of auxiliary gates and reduce the depths of output circuits by 11.76% on average in the initialization of the mapping, and TST has a better scalability than many state-of-the-art algorithms for adjusting mappings.

Keywords: Quantum circuit transformation · subgraph isomorphism · initial mapping · Tabu search

1 Introduction

Quantum technology has been applied in practice, but large quantum computers have not yet been built. Most of the contributions of quantum information to computer science are still in the theoretical stage. In 2017, IBM developed the first 5-qubit backend called IBM QX2, followed by the 16-qubit backend IBM QX3. The revised versions of them are called IBM QX4 and IBM QX5, respectively. IBM Q Experience provides the public with free quantum computer resources on the cloud and opens source the quantum computing software framework *Qiskit* [?].

Users of these early quantum computers mainly rely on quantum circuits to implement quantum algorithms. They design logical circuits which then go through the step of circuit transformation in order to map logical qubits to

^{*} Supported by organization x.

physical ones before the logical circuits are executed in physical devices. A big challenge for quantum information is the problem of quantum decoherence. Due to the decoherence of qubits, quantum gates need to be applied in a coherent period as the time for a qubit to stay in a coherent state is very short. For example, the longest coherence time of a superconducting quantum chip is still within 10us-100us, the duration of a single quantum gate is about 20ns, the duration of a 2-qubit gate is about 40ns, and the duration of a measurement operation is about 300ns-1us. The entanglement of a quantum system with its surrounding environment will lead to quantum decoherence. It is unrealistic to use quantum error correction in the circuit mapping process, since there are only dozens of available qubits for quantum devices in the NISQ era [16]. It is necessary to transform circuits by adding auxiliary gates to satisfy both logical and physical constraints, since quantum algorithms do not consider any hardware connectivity constraints. Hence, quantum circuit transformation is an important part of quantum circuit compilation. We need a set of highly efficient and automatic mapping procedures and adjustment routines to perform circuit transformation. In this process noise may be introduced, which brings a huge challenge to circuit compilation because noise has a significant impact on the final circuit and may make the result meaningless.

Paler [15] has shown that the initial mapping has an important influence on quantum circuit transformation. He has proposed a heuristic method to find the initial mapping and IBM's compiler for benchmark. Just by placing qubits in different positions from the default (trivial placement) in the actual circuit instance on the actual NISQ device, the time cost can be reduced by up to 10%. Li et al. [9] have proposed a novel reverse traversal technique, which determines the initial mapping by considering the entire circuit. Zhou et al. [23] have put forward an annealing algorithm to find an initial mapping, but it is unstable. In [10], Li et al. have considered the subgraph isomorphism algorithm *VF2* to generate an initial mapping.

The goal of circuit transformation algorithm is to find a minimum number of *SWAPs*. There are currently five main methods for solving the quantum circuit transformation problem.

Unitary matrix factorization algorithm. It is used in [8, 14] to rearrange the quantum circuit from the beginning while retaining the input circuit.

Converting into some existing problems. This approach converts the quantum circuit transformation problem into some existing problems, such as AI planning [22, 3], Integer Linear Programming (ILP) [1], or Satisfiability Modulo Theory (SMT) [12]. Existing tools for those problems are then used to find acceptable results. The approach cannot take advantage of certain properties of quantum mapping, which is a drawback. Furthermore, as the time cost is usually long, it can only deal with small-scale quantum circuits.

Exact methods. Siraichi et al. [19] have proposed an exact method, but it is only suitable for simple quantum architecture and cannot be extended to complex quantum architectures.

Graph theory. In [17], Shafaei et al. have used the minimum linear permutation problem in graph theory to model the problem of reducing the interaction distance. The idea is to first divide a given circuit into several subcircuits and apply the minimum linear permutation problem, respectively. Then we turn non-adjacent gates in the subcircuits into adjacent gates by adding auxiliary gates. Finally, we can use the minimum linear permutation problem to find an appropriate permutation and use bubble sort to calculate the number of necessary *SWAP* gates. In [7, 11], a two-step method is used to reduce the quantum circuit transformation to the graph problem to minimize the number of auxiliary gates, based on the graph coloring problem and the largest subgraph isomorphism problem.

Heuristic search. Heuristic search uses an evaluation function to obtain an acceptable solution in exponential time. Zulehner [] suggests to layer the circuits, group the circuits that could be executed in parallel into the same layer, and then determine compatible mappings for each of these layers to add as few auxiliary gates as possible. Zhou et al. [23] have designed a heuristic search algorithm with a novel selection mechanism. Instead of choosing the operation with the lowest cost to apply, one can look forward one step and then choose the best continuous operation. In this way, the algorithm can effectively avoid local minimum. Moreover, a pruning mechanism is introduced to reduce the search space’s size and ensure that the program terminates in a reasonable amount of time.

Li et al. [9] have proposed a *SWAP*-based search algorithm *SABRE*. Compared with previous search algorithms based on exhaustive mapping, *SABRE* ensures the scalability of *SABRE* to adapt to large quantum circuits in the NISQ era. In [4], a routing algorithm implemented in $t|ket\rangle$ ensures that any quantum circuit can be compiled into any architecture. The algorithm is divided into four stages: decomposing the input circuit into time steps, determining the initial mapping, routing across time steps, and finally cleaning up. The heuristics in $t|ket\rangle$ give the same or better results than other circuit transformation systems in terms of the depth and the total number of gates in the compiled circuit, with much shorter running time, and can handle larger circuits. In [21], a variation-aware qubit movement strategy is proposed. It takes advantage of the change in error rate and a change-aware quantum circuit transformation strategy by trying to select the route with the lowest probability of failure. This strategy uses the error rate of *SWAP*s to allocate logical qubits to physical qubits, thus avoiding paths with high error rates as much as possible.

In the current work, we adjust the lifetime of qubits through parallelization, and use *SubgraphCompare* to generate partial isomorphic subgraphs of logical circuits and physical circuits as part of the initial mapping. The advantage of the initial mapping result is that we use the appropriate subgraph isomorphism and the two-way connection of the logical circuit and the physical circuit to obtain a dense initial mapping, which avoids certain nodes from being mapped to remote locations. We use Tabu Search [6] to generate circuits that can be executed on physical devices. Tabu Search can avoid falling into local optimum

and swapping the recently swapped qubits, thereby improve the parallelism of quantum gates. We add the *SWAPs* associated with the gates on the shortest path to the candidate set, which greatly reduces the search space and improves the search speed. Our heuristic function not only considers the current gates but also the constraints of the gates already considered. The main contributions of this paper are as follows.

1. We propose a combined subgraph isomorphism algorithm (*CSI*) to generate part of the initial mapping and then complete the mapping based on the connectivity between qubits.
2. We propose a heuristic circuit transformation algorithm based on Tabu Search (*TST*) [6], which can handle large circuits in a shorter time at a lower cost, compared with existing precise search and heuristic algorithms.
3. We propose a look-ahead heuristic function that considers both the current gates and the gates to be processed. It filters out a swap that is beneficial to the current gates and also brings closer the gates to be processed.

The rest of this paper is organized as follows. In Section 2 we recall some background of quantum computing and quantum information. In Section 3 we introduce the problem of the transformation of quantum circuits. In Section 4 we describe and analyze our algorithm in detail. The experimental results are reported in Section 5. The last section concludes the paper and discusses some future research.

2 Background

This section introduces some notions and notations of quantum computing and quantum information.

Qubits Classical information is stored in bits, while quantum information is stored in qubits. Besides two basic states $|0\rangle$ and $|1\rangle$, a qubit can be in any linear superposition state like $|\phi\rangle = a|0\rangle + b|1\rangle$, where $a, b \in \mathbb{C}$ satisfy the condition $|a|^2 + |b|^2 = 1$. The intuition is that $|\phi\rangle$ is in the state $|0\rangle$ with the probability $|a|^2$ or in the state $|1\rangle$ with the probability $|b|^2$. We use letters in different fonts, e.g., q and q , to represent a physical qubit and a logical qubit, respectively.

Quantum Gates In order to change the state of a quantum system, we apply quantum gates. Some commonly used quantum gate symbols and their semantics in terms of matrices are shown in Figure. 1.

Quantum Circuit A quantum logical circuit LC consists of quantum gates interconnected by quantum wires [5]; see Figure 2 for an example. A quantum wire is a mechanism for moving quantum data from one location to another. Each line represents a qubit, and the gates on the lines act on the corresponding qubits. The execution order of a quantum logical circuit is from left to right. The

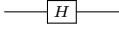
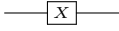
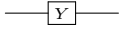
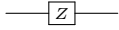
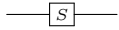
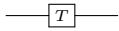
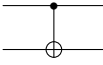
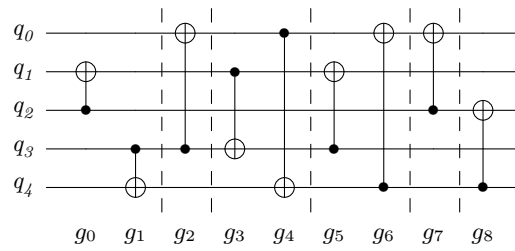
Hadamard gate		$\frac{1}{\sqrt{2}} \begin{bmatrix} 1 & 1 \\ 1 & -1 \end{bmatrix}$
Pauli-X gate		$\begin{bmatrix} 0 & 1 \\ 1 & 0 \end{bmatrix}$
Pauli-Y gate		$\begin{bmatrix} 1 & -i \\ i & 0 \end{bmatrix}$
Pauli-Z gate		$\begin{bmatrix} 1 & 0 \\ 0 & -1 \end{bmatrix}$
phase gate		$\begin{bmatrix} 1 & 0 \\ 0 & i \end{bmatrix}$
$\frac{\pi}{8}$ gate		$\begin{bmatrix} 1 & 0 \\ 0 & e^{i\pi/4} \end{bmatrix}$
<i>CNOT</i> gate		$\begin{bmatrix} 1 & 0 & 0 & 0 \\ 0 & 1 & 0 & 0 \\ 0 & 0 & 0 & 1 \\ 0 & 0 & 1 & 0 \end{bmatrix}$

Fig. 1. The symbols of common quantum gates and their matrices

width w of a circuit refers to the number of qubits in the circuit. The depth d of a circuit refers to the number of layers executing in parallel. For example, the depth of the circuit in Figure 2 is 6, and the width is 5. In this paper, a circuit with a depth less than 100 is called a small-scale circuit, a circuit with a depth greater than 1000 is called a large-scale circuit, and the rest are medium-scale circuits. It is unnecessary to consider quantum gates acting on single qubits in circuit transformation, since the single qubits are *local* [18].

**Fig. 2.** Original circuit

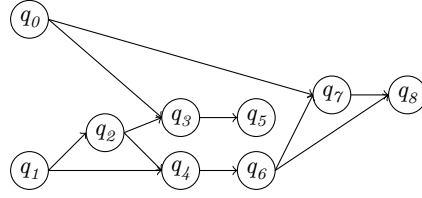


Fig. 3. The directed acyclic graph (*DAG*) of original circuit in Fig. 2

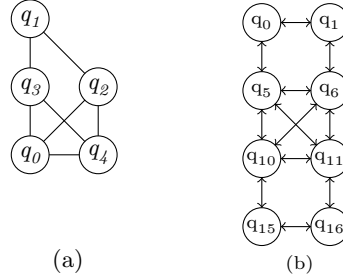


Fig. 4. (a) The architecture graph of original circuit in Fig. 2. (b) The partial architecture graph of IBM Q20.

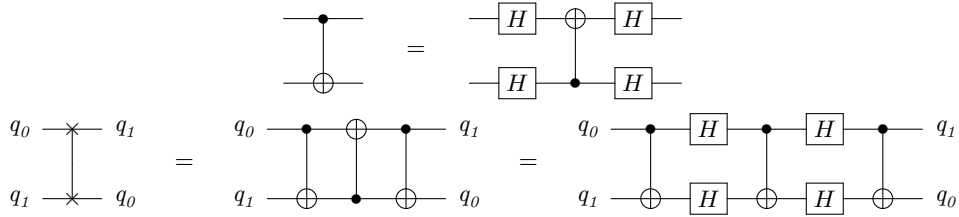


Fig. 5. The above circuit changes the direction of the *CNOT* gate by adding four H gates, and below is the circuit of the *SWAP* gate.

Architectures We mainly discuss the physical circuits of IBM Q series. Let $\mathcal{AG}_{\mathcal{P}} = (V_{\mathcal{P}}, E_{\mathcal{P}})$ denote the architecture graph of the physical circuit, where $V_{\mathcal{P}}$ denotes the set of physical qubits and $E_{\mathcal{P}}$ denotes the set of edges that connect *CNOT* gates. In Figure 6, diagrams (a) and (b) are the physical architecture graphs (PAG) of the 5-qubit IBM QX2 and IBM QX4, respectively. Diagrams (c) and (d) are the PAGs of the 16-qubit IBM QX3 and IBM QX5, respectively, and diagram (e) is the PAG of IBM Q20. The direction in each edge indicates the control direction of a 2-qubit gate, and 2-qubit gates can only be performed between qubits with edges connected. IBM physical circuits only support single quantum gates and *CNOT* gates between two adjacent qubits.

Given a logical circuit LC , a physical structure \mathcal{AG}_P , an initial mapping τ , and a $CNOT$ gate $g = \langle q_i, q_j \rangle$, where q_i is the control qubit, q_j is the target qubit. If gate g is executable on a physical circuit, then $\langle \tau(q_i), \tau(q_j) \rangle$ must be a directed edge on \mathcal{AG}_P .

Example 1. Figure 4 (a) is the logical structure of Figure 2. Figure 4 (b) is the partial architecture graph of IBM Q20. An initial mapping is

$$\tau = \{q_0 \rightarrow q_{10}, q_1 \rightarrow q_0, q_2 \rightarrow q_6, q_3 \rightarrow q_5, q_4 \rightarrow q_{11}\}.$$

The 2-qubit gate $g_0 = \langle q_2, q_1 \rangle$ is not executable, since the edge $\langle \tau(q_2), \tau(q_1) \rangle = \langle q_6, q_0 \rangle$ does not exist in \mathcal{AG}_P . But $g_3 = \langle q_1, q_3 \rangle$ is executable, since the edge $\langle \tau(q_1), \tau(q_3) \rangle = \langle q_0, q_5 \rangle$ exists in \mathcal{AG}_P .

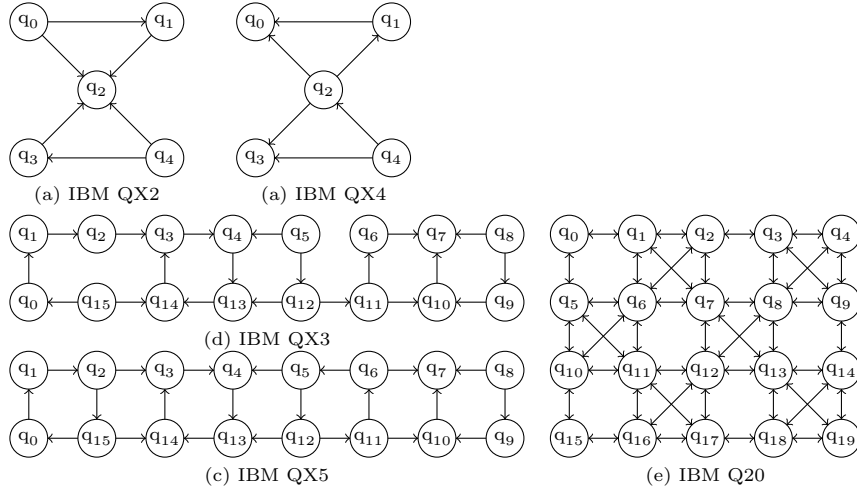


Fig. 6. IBM QX architectures

3 Problem Analysis

Single qubit gates and $CNOT$ gates are used as basic gates, since they are commonly used to implement any quantum circuit supported by the IBM QX architecture. Before circuit transformation, a circuit should be simplified to have only single quantum gates and $CNOT$ gates [13, 2]. We insert auxiliary gates (see Figure 5) to move two non-adjacent quantum positions to adjacent positions or change the direction of a $CNOT$ gate, but this process may introduce errors. We hope to find a circuit transformation algorithm that can produce the output circuit with a minimal number of auxiliary gates and a small circuit depth in an acceptable amount of time. A quantum circuit transformation

mainly includes the following four steps. Isomorphism and transformation are both NP-complete [19].

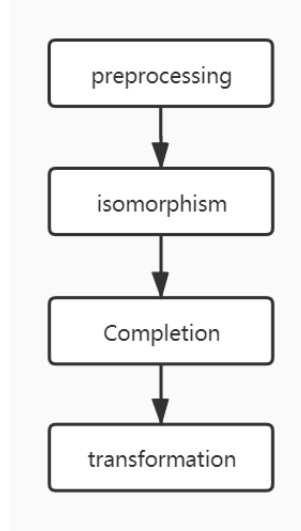


Fig. 7. Circuit transformation process

1. *Preprocess the logical quantum circuit.* This step includes extracting the logical architecture graph (*LAG*) of the circuit, adjusting the life cycle of qubits as done in [24]), and calculating the shortest paths of the physical circuit.
2. *Compute isomorphic substructures.* This step uses the subgraph isomorphism algorithm to find part of the initial mappings as done in [20].
3. *Generate a high-quality initial mapping.* In this step we perform a mapping completion to include the remaining nodes that do not satisfy all isomorphism requirements, according to the connectivity between the unmapped node and the mapped nodes. Unmapped nodes are mapped to the neighborhood of mapped nodes, which satisfies the connectivity of part of the *LAG* and *PAG* and reduces the length of the shortest path.
4. *Transforming logical circuits to meet physical constraints.* Circuit transformation need to be performed before compiling quantum circuits, since the design of quantum algorithms usually does not refer to the connectivity constraints of any hardware. Therefore, it is indispensable for any quantum compiler.

4 Solution

Our solution mainly includes preprocessing, initial mapping, and circuit transformation. In this section, we will introduce them in detail.

4.1 Preprocessing

Before a circuit transformation, we can preprocess it to collect more data so as to shorten our search time and space. In the preprocessing step, we adjust the input circuit described by an openQASM program to shorten the life cycle of qubits. Then we use Breadth-First Search (BFS) to calculate the shortest distance between each node on the architecture graph.

Circuit Adjustment We use a layered method to analyze the life cycle of qubits and pack the gates that can be executed in parallel into a *bundle*, forming a layered bundle format [24]. A conversion method is designed to use the layered bundle format to determine which gates can be moved, which reduces the life cycle of these qubits. The algorithm reduces the error rate of quantum programs by 11% on average. In most quantum workloads, the longest qubit lifetime and the average qubit lifetime can be reduced by more than 20%, and the execution time of some quantum programs can also be reduced.

Shortest Distance Given a *PAG* and assume the distance of each edge is 1, we can use *Floyd-Warshall* algorithm to calculate the shortest distance matrix $dist[i][j]$, which represents the shortest distance from q_i to q_j .

For IBM QX2, QX3, QX4, QX5, a *SWAP* needs 7 gates (3 *CNOT* gates and 4 *H* gates). Only 4 *H* gates are needed to change the direction of an adjacent *CNOT* gate. For a *CNOT* gate $g = \langle q_i, q_j \rangle$, the two qubits are mapped to q_m and q_n , respectively, with $\tau(q_i) = q_m, \tau(q_j) = q_n$. Then the cost of executing g under the shortest distance path is $cost_{cnot}(q_i, q_j) = 7 \times (dist[m][n] - 1)$. For IBM Q20, in which all edges are bidirectional, a *SWAP* requires 3 *CNOT* gates. Thus the cost between them is $cost_{cnot}(q_i, q_j) = 3 \times (dist[m][n] - 1)$. The time complexity is $O(N^3)$.

Example 2. Take the QX5 structure as an example. Suppose there is a *CNOT* gate $g = \langle q_i, q_j \rangle$, q_i is mapped to q_1 , q_j is mapped to q_{14} , and the shortest distance between them is $dist[1][14] = 3$. There are 3 shortest paths to move q_1 to the adjacent position of q_{14} : $\Pi = \{\pi_0, \pi_1, \pi_2\}$, $\pi_0 = q_1 \rightarrow q_2 \rightarrow q_3 \rightarrow q_{14}$, $\pi_1 = q_1 \rightarrow q_2 \rightarrow q_{15} \rightarrow q_{14}$, $\pi_2 = q_1 \rightarrow q_0 \rightarrow q_{15} \rightarrow q_{14}$. Their costs are $cost_{\pi_0} = 18$, $cost_{\pi_1} = 14$, $cost_{\pi_2} = 14$, respectively.

Circuit Layering Quantum gates acting on different qubits can be executed in parallel. Therefore, we classify the gates that can be executed in parallel into one layer, otherwise we add a new layer. The notation $L(LC) = \{\mathcal{L}_0, \mathcal{L}_1, \dots, \mathcal{L}_n\}$ represents the layered circuit, where \mathcal{L}_i ($0 \leq i \leq n$) stands for a quantum gate set that can be executed in parallel. The quantum gate set separated by the dotted line in Figure 2 are the following $\mathcal{L}_0 = \{g_0, g_1\}, \mathcal{L}_1 = \{g_2\}, \mathcal{L}_2 = \{g_3, g_4\}, \mathcal{L}_3 = \{g_5, g_6\}, \mathcal{L}_4 = \{g_7\}, \mathcal{L}_5 = \{g_8\}$.

At the same time, we generate logical circuit architecture graph $\mathcal{AG}_{\mathcal{L}} = (V_L, E_L)$, which is an undirected graph with V_L containing the vertices and the

degree of each vertex, and E_L representing the set of undirected edges that the *CNOT* gates can execute.

4.2 Initial Mapping

We use the subgraph isomorphism algorithm to find a partial initial mapping that helps to minimize auxiliary gates added by the output circuit.

In a *PAG*, it is almost impossible to find a subgraph that exactly matches all the nodes in a *LAG*. Thus, we regard the mapping with the largest number of matching nodes as the partial mapping. *SubgraphCompare* [20] compares several state-of-the-art subgraph isomorphism algorithm compositions. It shows that the best performance can be achieved by using filters and the sorting ideas of the *GraphQL* algorithm to process candidate nodes, and the local candidates calculation method *LFTJ* based on set-intersection to enumerate the results. We artificially connect the isolating qubits to the qubits with the largest degree in the logical architecture graph, since *SubgraphCompare* cannot handle disconnected graphs. We would like to minimize the impact of logical dependency graphs, thus map isolated nodes to nodes with the largest degree.

The input of Algorithm 1 is a target graph (\mathcal{AG}_P), a query graph (\mathcal{AG}_L), and the partial mappings T . First, we initialize an empty queue Q . Then we traverse τ and add the unmapped nodes to the queue Q . For the unmapped nodes, we try to map them to the vicinity of the mapped nodes in \mathcal{AG}_P . Finally, we generate a dense mapping, which can reduce the added auxiliary gates. We could try to match the remaining unmapped nodes randomly, but it may lead to a mapping with a node far away from other nodes. If an unmapped node has an edge adjacent to a matched node in the query graph, it will be matched to one of the adjacent nodes first. In this way, we can obtain all initial candidate mappings.

In Algorithm 1, line 2 selects the partial mapping with the most mapped nodes l as the candidate set. Lines 3-40 complete the partial mapping. In line 6, we initialize an empty queue Q , which stores unmapped logical qubits. In lines 8-13, we traverse the mapping τ and add the unmapped qubits to Q . We iterate the loop until Q is empty, and all logical qubits are mapped to physical qubits. We take out the first element in Q to q . Lines 16-17 are used to get the adjacency matrices of \mathcal{AG}_P and \mathcal{AG}_L , respectively. Line 18 initializes an empty map *cans*, sort by a descending order of whether q_m is mapped and the number of gate appearances. Lines 20-22 store the nodes q_m connected to q in the adjacency matrix in *cans*. Lines 23-38 traverse *cans*, select the node q_m that has been mapped to the node (*cans.first*) on *PAG*, and has the largest number of connections to q in *cans*, with q being the node that q_m is mapped to in τ . Line 26 deletes the node from *cans*. Lines 27-34 select the node k adjacent to q in the adjacency matrix, and maps q to that node.

Example 3. Following the previous example, we first use the *CSI* algorithm for the *LAG* given in Figure 4 (a) and the *PAG* given in Figure 6 (e) to obtain the partial mapping set $T = \{\tau_0, \tau_1, \dots, \tau_n\}$. Then we use one of the partial mappings

Algorithm 1: Initial mapping algorithm *CSI*

Input: $\mathcal{AG}_{\mathcal{L}}$: The architecture of logical circuit
 $\mathcal{AG}_{\mathcal{P}}$: The architecture of physical circuit
 T : A partial mapping set obtained by *SubgraphCompare*
Output: *result*: A collection of mapping relations between $\mathcal{AG}_{\mathcal{L}}$ and $\mathcal{AG}_{\mathcal{P}}$

```

1 Initialize result =  $\emptyset$  ;
2  $l \leftarrow \max_{\tau \in T} \tau.length$ ;
3 for  $\tau \in T$  do
4   if  $l = \tau.length$  then
5     result.add( $\tau$ );
6      $Q \leftarrow$  initialing an empty unmapped node queue
7      $i \leftarrow 1$ ;
8     while  $i \leq \tau.length$  do
9       if  $\tau[i] = -1$  then
10         $Q \leftarrow i$ ;
11      end
12       $i \leftarrow i + 1$ ;
13    end
14    while  $Q$  is not empty do
15       $q \leftarrow Q.poll()$ ;
16       $targetAdj \leftarrow \mathcal{AG}_{\mathcal{P}}.adjacencyMatrix()$ ;
17       $queryAdj \leftarrow \mathcal{AG}_{\mathcal{L}}.adjacencyMatrix()$ ;
18       $cans \leftarrow$  initialing an empty candidate node list ;    // sorted by
        the connectivity of nodes
19      foreach  $q_m \leq queryAdj[q].length$  do
20         $cans \leftarrow cans \cup \{q_m\}$ ;
21      end
22      while  $cans$  is not empty do
23         $q \leftarrow \tau[cans.first]$ ;
24         $k \leftarrow 0$ ;
25         $cans \leftarrow cans \setminus cans.first$ ;
26        while  $k < targetAdj[q].length$  do
27          if ( $targetAdj[q][k] \neq -1$  or  $targetAdj[k][q] \neq -1$ )
28            and not  $\tau.contains(k)$  then
29             $\tau[q] \leftarrow k$ ;
30            break;
31          end
32           $k \leftarrow k + 1$ ;
33        end
34        if  $k \neq targetAdj[q].length$  then
35          break;
36        end
37      end
38    end
39  end
40 end

```

as an example. $\tau_0 = \{q_0 \rightarrow q_{10}, q_1 \rightarrow -1, q_2 \rightarrow q_6, q_3 \rightarrow q_5, q_4 \rightarrow q_{11}\}$, $0 \leq i < n$. Here $q_1 \rightarrow -1$ means that q_1 is not mapped to any physical node, so we need to perform a mapping completion. In this example, the maximum number of mapped nodes is 4. Next, we demonstrate how τ_0 is completed. We add all unmapped nodes to the queue Q , $Q = \{q_1\}$, and end the loop ends when Q is empty. We put the first element of Q into q , and delete it from Q . Then we get the adjacency matrix of the query graph and the target graph, and traverse the adjacency matrix. We put the nodes q_m adjacent to q into the candidate nodes list *cans*, which is sorted by the connectivity of q_m and q . We get *cans* = $\{q_3, q_2, q_4, q_0\}$. Thereafter, we traverse *cans* and take out of the first element *value* = q_3 in *cans*, and calculate the physical node $q = q_5$, $\tau_0(q_3) = q_5$. Finally, we map q to the node connected to q but not yet mapped. If the nodes connected to q have been mapped, the loop continues. In this example, it can be directly mapped to q_0 . In the end, we obtain the mapping

$$\tau_0 = \{q_0 \rightarrow q_{10}, q_1 \rightarrow q_0, q_2 \rightarrow q_6, q_3 \rightarrow q_5, q_4 \rightarrow q_{11}\}.$$

4.3 Swap Minimization

Tabu Search The Tabu Search algorithm is a type of heuristic algorithm. It uses a tabu list to avoid searching repeated spaces, thereby avoiding deadlock. The algorithm uses amnesty rules to jump out of the local optimum to ensure the diversity of transformed results. The circuit transformation mainly relies on the Tabu Search algorithm, aiming to deal with those large-scale circuits that the current algorithm is difficult to handle and produce a output circuit closer to the optimum solution in a short time.

The following objects are defined in Tabu Search: neighborhood field, neighborhood action, tabu list, candidate set, tabu object, evaluation function, and amnesty rule. All the edges that can be swapped in the current map are the neighborhood fields. The tabu list avoids local optimum and guarantees the parallelism of auxiliary gates. The tabu object is the object in the tabu list. We try not to use the recently swapped qubits as much as possible, which are added to the tabu list. We perform pruning to save search space, because only swaps adjacent to at least one gate node are meaningful. We select the edge in the shortest path that has an intersection with the qubits contained in the gate as the candidate set. The evaluation function selects a *SWAP* evaluation formula from the candidate set, taking the objective function as the evaluation function in general. The evaluation function satisfies some gates, and the number of *SWAP* gates added or the depth of the entire circuit should be small. The amnesty rules are used when all objects in the candidate set are banned, or after banning an object, the target value will be greatly reduced.

The calculation of the neighborhood fields is shown in Algorithm 2. The input is the current circuit mapping τ_p . The variable *qubits* contains the mapping of physical qubits to logical qubits, where $j = \text{qubits}[i]$ means that the i -th physical qubit has been mapped to the j -th logical qubit. The variable *locations* represents the mapping of logical qubits to physical qubits, where $j = \text{locations}[i]$

means that the i -th logical qubit has been mapped to the j -th physical qubit. The current layer list of all gates is cl , and the output is a candidate set of the current mapping. The set E contains the edges of all the shortest paths in the physical architecture graph of all the gates in the current layer. Lines 17-37 swap all the edges of candidate set, and calculate the cost of them.

Example 4. Let us consider the mapping

$$\tau_0 = \{q_0 \rightarrow q_{10}, q_1 \rightarrow q_0, q_2 \rightarrow q_6, q_3 \rightarrow q_5, q_4 \rightarrow q_{11}\},$$

for $L_0 = \{g_0, g_1\}$, $dist_{cnot}(g_0) = 3$ and $dist_{cnot}(g_1) = 3$. Gate g_1 can be executed directly in the τ_0 mapping, so we delete it from L_0 , but g_0 cannot be executed in the mapping τ_0 . Thus, a circuit transformation is required. Nodes that cannot be executed join the set $swap_nodes = \{q_0, q_6\}$. The set of shortest paths is $paths = \{\{q_6 \rightarrow q_1 \rightarrow q_0\}, \{q_6 \rightarrow q_5 \rightarrow q_0\}\}$, and then we traverse the shortest paths to calculate the candidate set. The two endpoints of an edge passed by one of the shortest paths should intersect the swap set and join the candidate set. The current candidate set is $\{SWAP(q_6, q_1), SWAP(q_1, q_0), SWAP(q_6, q_5), SWAP(q_5, q_0)\}$.

The circuit mapping algorithm based on Tabu Search takes a layered circuit and an initial mapping as input and outputs a circuit that can be executed in the specified architecture graph (see Algorithm 3). The transformed circuit mapping of each layer is used as the initial mapping of the next layer of the circuit. Lines 2-3 regard the initial mapping τ_{ini} as the best mapping τ_{best} and the current mapping is τ_{curr} . Lines 4-17 cyclically check whether all gates in the current layer can be executed under the mapping τ_{curr} . If not all the gates are executable or the number of iterations has not reached the given maximum number, the search will continue. Otherwise, the search will terminate. Line 5 gets the current mapping candidate, and Line 6 finds the best mapping in the candidate set. The mapping will first remove the overlapping elements of the candidate set and the tabu list. Then from the remaining candidates, we choose a mapping with the lowest cost. Lines 7-12 are the amnesty rules. When the best candidate is not found, the candidate set elements are all the same as the tabu list elements. The amnesty rules select the mapping with the lowest cost in the candidate set as the best candidate mapping. Lines 13-16 update the best mapping τ_{best} and the current mapping τ_{curr} , and add the $SWAP$ performed by the best mapping to the tabu list tl , indicating that the $SWAP$ has just been performed. The algorithm would try to avoid re-swapping the just swapped qubits. Then it will judge whether the termination condition of the algorithm is satisfied. The condition determines whether the number of iterations has reached the maximum number, or the current mapping ensures all gates in the current layer can be executed.

Example 5. Let us continue the previous example. We start searching from the initial mapping. We need to get the candidate $SWAP$ set and select the one with the lower evaluation scores. For $L_0 = \{g_0, g_1\}$, the candidate set is

$$\{SWAP(q_6, q_1), SWAP(q_1, q_0), SWAP(q_6, q_5), SWAP(q_5, q_0)\},$$

Algorithm 2: Calculate the candidate sets

Input: *dist*: The shortest paths of physical architecture
qubits: The mapping from physical qubits to logical qubits
locations: The mapping from logical qubits to physical qubits
cl: Gates included in the current layer of circuits
Output: *results*: The set of candidate solution

```

1 Initialize results  $\leftarrow \emptyset$ ;
2  $E_w \leftarrow$  Calculate the weight of each edge
3 swap_nodes  $\leftarrow$  An empty set of candidate swap nodes
4 foreach  $g \in cl$  do
5    $q_1 \leftarrow locations[g.control]$ ;
6    $q_2 \leftarrow locations[g.target]$ ;
7   if  $g$  is executable then
8      $cl \leftarrow cl \setminus g$ ;
9     continue;
10  end
11  swap_nodes.add( $q_1$ );
12  swap_nodes.add( $q_2$ );
13 end
14 foreach  $g \in cl$  do
15    $q_1 \leftarrow locations[g.control]$ ;
16    $q_2 \leftarrow locations[g.target]$ ;
17   foreach  $path \in paths[q_1][q_2]$  do
18     foreach  $e \in path$  do
19       if swap_nodes.contains(sour_node) or
        swap_nodes.contains(tar_node) then
20          $new\_qubits \leftarrow qubits$ ;
21          $new\_locations \leftarrow locations$ ;
22          $q_1 \leftarrow new\_qubits[e.source]$ ;
23          $q_2 \leftarrow new\_qubits[e.target]$ ;
24          $new\_qubits[e.source] \leftarrow q_2$ ;
25          $new\_qubits[e.target] \leftarrow q_1$ ;
26         if  $q_1 \neq -1$  then
27            $new\_locations[q_1] \leftarrow q_2$ ;
28         end
29         if  $q_2 \neq -1$  then
30            $new\_locations[q_2] \leftarrow q_1$ ;
31         end
32          $s \leftarrow \emptyset$ ;
33          $s.value \leftarrow compute\_evaluate\_value(dist, new\_locations, cl)$ ;
34          $results \leftarrow results \cup s$ ;
35       end
36     end
37   end
38 end
39 return results;

```

and the costs are as follows.

$$\begin{aligned} \text{cost}(\text{SWAP}(q_6, q_1)) &= 3.0, & \text{cost}(\text{SWAP}(q_1, q_0)) &= 3.0, \\ \text{cost}(\text{SWAP}(q_6, q_5)) &= 3.0, & \text{cost}(\text{SWAP}(q_5, q_0)) &= 3.0. \end{aligned}$$

The algorithm will choose the first *SWAP*, the mapping becomes

$$\tau_0 = \{q_0 \rightarrow q_{10}, q_1 \rightarrow q_0, q_2 \rightarrow q_1, q_3 \rightarrow q_5, q_4 \rightarrow q_{11}\}.$$

It can be seen that the current mapping ensures the executability of g_0 . The algorithm continues to search for the next layer.

Algorithm 3: Tabu Search

Input: τ_{ini} : The initial mapping
 tl : Tabu list
Output: τ_{best} : The final state and *SWAPs*

```

1 Initialize  $\tau_{best} \leftarrow \tau_{ini}$ ;
2  $\tau_{curr} \leftarrow \tau_{ini}$  ;
3  $iter \leftarrow 1$  ;                                     // Number of iterations
4 while not mustStop( $iter, \tau_{best}$ ) do
5    $C \leftarrow \tau_{curr}.candidates()$  ;                 // candidate set
6    $C_{best} \leftarrow find\_best\_candidates(C, tl)$ ;
7   if  $C_{best}$  is empty then
8     if  $C = NULL$  then
9       break;
10    end
11     $C_{best} \leftarrow find\_amnesty\_candidates(C, tl)$ ;
12  end
13   $\tau_{best} \leftarrow C_{best}$ ;
14   $\tau_{curr} \leftarrow C_{best}$ ;
15   $tl \leftarrow tl \cup \{C_{best}.swap\}$  ;
16   $iter \leftarrow iter + 1$ ;
17 end
18 return  $\tau_{best}$ 

```

Evaluation functions We can control the search direction by changing the evaluation functions. We test two evaluation functions: one uses the number of auxiliary gates in the generated circuit as the evaluation criterion (1), and the other uses the depth of the generated circuit as the evaluation criterion (2).

$$\text{cost}(\text{SWAP}(q_m, q_n)) = \sum_{g \in L_i} (\text{dist}[g.control][g.target]) \quad (1)$$

$$\text{cost}(\text{SWAP}(q_i, q_j)) = \text{Depth}(L_i) \quad (2)$$

Here $\text{cost}(\text{SWAP}(q_i, q_j))$ represents the cost of executing all the gates of the current layer L_i after swapping q_i with q_j . We only calculate the depth between the unmapped gates as in (1) or the distance of the unmapped gates as in (2).

Look ahead We observe that the number of gates in each layer after layering is small. The output of the i -th ($i < n$) layer is used as the input of the $(i+1)$ -th layer. Note that any swap operation in the i -th layer will affect the mapping of the $(i+1)$ -th layer. If we only consider the gates in the current layer when choosing the swapping gates, the swap only satisfies the requirement of the i -th layer, not necessarily the next layer. Therefore, we take the gates in the $(i+x)$ -th ($i+x < n$) layer into consideration. However, it is necessary to give a higher priority to the execution of the gates in the i -th layer, so we introduce an attenuation factor δ , which controls the influence of the gates in the $(i+x)$ -th layer. Heuristics show that for $x = 2$, $\delta = 0.9$, the final effect is approximately the best. Our evaluation functions in (1) and (2) can be adjusted as (3) and (4), respectively.

$$\begin{aligned} cost(SWAP(q_m, q_n)) = & \sum_{g \in L_i} (dist[g.control][g.target]) + \\ & \delta \times \sum_{j=i}^{i+x} \sum_{g \in L_j} (dist[g.control][g.target]) \end{aligned} \quad (3)$$

$$cost(SWAP(q_m, q_n)) = Depth(L_i) + \delta \times Depth\left(\sum_{j=i}^{i+x} L_j\right). \quad (4)$$

Complexity Given a logical circuit architecture graph $\mathcal{AG}_L = (V_L, E_L)$ and a physical circuit architecture graph $\mathcal{AG}_P = (V_P, E_P)$, we assume that the initial mapping is τ , the depth of the circuit is d , and the number of qubits is V_L . Tabu Search deals with one layer at a time, and searches at most d times. Starting from the initial mapping, we first delete the executable gates of the first layer under the initial mapping. Then, the edges of all the shortest paths of all the gates that are not executable in the current layer are added to the candidate set where at least one node is in the gate mapping. In the worst case, the length of the shortest path is $(|E_P| - 1)$ and the size of the candidate set is $(|E_P| - 1)$. Each *SWAP* will make the total distance between the gates smaller. In the worst case, the number of *SWAPs* is $(|E_P| - 1)^{|E_P| - 2}$, but our selection strategy will make the number of *SWAPs* significantly reduced. Our time complexity is $d * ((|E_P| - 1))^{(|E_P| - 2)}$, and the space complexity is the size of our candidate set $(E_P - 1)$.

5 Experiments

We compare the *CSI* algorithm and the circuit transformation algorithm based on Tabu Search *TST* with the *wghtgraph* in [10] and the heuristic algorithm *A** in [25]. All the experiments are conducted on a Linux machine with 2.3GHz CPU and 64G memory.

First, we compare the efficiency of initial mapping on τ_{optm} [25], τ_{CSI} and $\tau_{wgtgraph}$ [10]. In order to observe the results of these two initial mapping algorithms, we used the same circuit transformation algorithm A^* [25]. We have tested 159 circuits. Within five minutes, τ_{optm} , $\tau_{wgtgraph}$, and τ_{CSI} can deal with 121, 106, and 131 circuits, respectively. There are 103 circuits that they can handle. We then compare the $\tau_{wgtgraph}$ algorithm and the τ_{CSI} algorithm more closely. The $\tau_{wgtgraph}$ algorithm has 21 circuits with fewer auxiliary gates and 19 circuits with smaller depths, and the τ_{CSI} algorithm has 54 circuits with fewer auxiliary gates and 60 circuits with smaller depths. They output 25 circuits with equal depth and 29 circuits with equal auxiliary gates. On average, the auxiliary gates of the τ_{CSI} algorithm are reduced by 22.44%, and the depths are reduced by 11.25%.

Next, we compare the τ_{optm} algorithm and the τ_{CSI} algorithm. The τ_{optm} algorithm has one circuit with fewer auxiliary gates and two circuits with a small depth, while the τ_{CSI} algorithm has 99 circuits with fewer auxiliary gates and 98 circuits with a small depth. They have 4 circuits with equal depths and 4 circuits with equal auxiliary gates. The auxiliary gates of the τ_{CSI} algorithm are relatively reduced by 27.02%, and the depths are reduced by 14.12%. Table 1 shows the experimental data on 104 circuits. The three initial mapping algorithms are compared according to the depths of the generated circuits using the same A^* algorithm, and the numbers of added auxiliary gates. The column headed by τ_{CSI}/τ_{optm} shows the efficiency improvement of the former upon the latter, e.e. $(n_{optm} - n_{CSI})/n_{optm}$.

	τ_{optm}	$\tau_{wgtgraph}$	τ_{CSI}	τ_{CSI}/τ_{optm}	$\tau_{CSI}/\tau_{wgtgraph}$
Depths	168895	163422	145040	14.12%	11.25%
Auxiliary gates	20439	19232	14916	27.02%	22.44%

Table 1. Compare τ_{optm} , $\tau_{wgtgraph}$, and τ_{CSI}

We then compare the use of two indicators TST_{dep} and TST_{num} that prioritize smaller depths and fewer auxiliary gates, respectively. Using the two indicators as objective functions, we tested 159 circuits. The depths of the final circuits obtained by TST_{num} are 1.93% smaller than TST_{dep} on average, and the numbers auxiliary gates added are 4.53% smaller on average. When inserting a *SWAP* gate, the circuit needs to add 3 *CNOT* gates, and the depth will be increased by 3. Therefore, if fewer *SWAP* gates are added, the depths of the circuits will reduce accordingly.

Finally, we compare TST and $wgtgraph$. Since the $wgtgraph$ algorithm only uses 2-qubit gates, it is impossible to compare the depths of the generated circuits. Instead, we compare the number of *SWAP* gates added and the time costs. We set a five-minute timeout period and tested 159 circuits. It turns out that TST_{num} only takes 461 seconds and TST_{dep} takes 485 seconds. The $wgtgraph$ algorithm takes 1908 seconds for the 159 circuits, but only produces valid results

for 98 circuits, including 66 small-scale circuits, 35 medium-scale circuits, and no circuit output is produced for any of the 44 large circuits. Although Tabu Search can quickly produce results on large circuits, in contrast, more auxiliary gates are added. In the generated circuits obtained by *wgtgraph* from 98 small-scale and medium-scale circuits, the number of *SWAP* gates added by *wgtgraph* is 26.87% (resp. 24.89%) smaller than TST_{num} (resp. TST_{dep}) on average. The Tabu Search can quickly output converted circuits on large circuits, but *wgtgraph* cannot get results in a short time. As to *SABRE*, when dealing with 159 circuits with a five-minute limit for each circuit, it successfully produces results for only 23 small-scale circuits, 6 medium-scale circuits, and 1 large circuit. The detailed results of the circuit comparisons are in the Appendix.

benchmarks	#circ.	TST_{num}		TST_{dep}		<i>wgtgraph</i>		<i>SABRE</i>	
		#succ.	time	#succ.	time	#succ.	time	#succ.	time
small	66	66	32	66	29	64	587	23	12996
medium	49	49	45	49	40	35	1183	6	13019
large	44	44	407	44	432	0	-	0	1340719
total	159	159	484	159	501	98	-	29	1366734

Table 2. Compare τ_{optm} , $\tau_{wgtgraph}$, and τ_{TST}

6 Conclusion

We proposes to use the combined subgraph isomorphism algorithm to generate high-quality initial mappings and a heuristic Tabu Search to perfrom circuit transformation. Experimental results show that the initial mappings generated by *CSI* have fewer *SWAP* gates inserted and the results can be obtained in a short time. Most small-scale and medium-scale circuits can be handled in a few seconds. For large-scale circuits, the results can be obtained within a few minutes, but the cost of insertion may be lareger than that of *wgtgraph*. We introduce a look-ahead method to make each selected *SWAP* more in line with the constraints of the gates to be processes. In the future, we will investigate how to reduce the number of auxiliary gates inserted but increase the speed. We will also apply the proposed method to more NISQ devices.

References

1. Almeida, A., Dueck, G., Silva, A.: Finding optimal qubit permutations for ibm’s quantum computer architectures pp. 1–6 (08 2019). <https://doi.org/10.1145/3338852.3339829>
2. Barenco, A., Bennett, C., Cleve, R., DiVincenzo, D., Margolus, N., Shor, P., Sleator, T., Smolin, J., Weinfurter, H.: Elementary gates for quantum computation. *Physical Review A* **52** (03 1995). <https://doi.org/10.1103/PhysRevA.52.3457>

3. Bernal, D., Booth, K., Dridi, R., Alghassi, H., Tayur, S., Venturelli, D.: Integer programming techniques for minor-embedding in quantum annealers (12 2019)
4. Cowtan, A., Dilkes, S., Duncan, R., Krajenbrink, A., Simmons, W., Sivarajah, S.: On the qubit routing problem (02 2019)
5. Daei, O., Navi, K., Zomorodi, M.: Optimized quantum circuit partitioning (05 2020)
6. Glover, F.: Tabu search—part ii. *ORSA Journal on Computing* **2**, 4–32 (02 1990). <https://doi.org/10.1287/ijoc.2.1.4>
7. Guerreschi, G.G., Park, J.: Two-step approach to scheduling quantum circuits. *Quantum Science and Technology* **3** (06 2018). <https://doi.org/10.1088/2058-9565/aacf0b>
8. Kissinger, A., Meijer, A.: Cnot circuit extraction for topologically-constrained quantum memories (04 2019)
9. Li, G., Ding, Y., Xie, Y.: Tackling the qubit mapping problem for nisq-era quantum devices (09 2018)
10. Li, S., Zhou, X., Feng, Y.: Qubit mapping based on subgraph isomorphism and filtered depth-limited search (2020)
11. Matsuo, A., Yamashita, S.: An efficient method for quantum circuit placement problem on a 2-d grid pp. 162–168 (05 2019). https://doi.org/10.1007/978-3-030-21500-2_10
12. Murali, P., Linke, N., Martonosi, M., Abhari, A., Nguyen, N., Huerta Alderete, C.: Full-stack, real-system quantum computer studies: architectural comparisons and design insights pp. 527–540 (06 2019). <https://doi.org/10.1145/3307650.3322273>
13. Möttönen, M., Vartiainen, J.: Decompositions of general quantum gates. *Frontiers in Artificial Intelligence and Applications* (05 2005)
14. Nash, B., Gheorghiu, V., Mosca, M.: Quantum circuit optimizations for nisq architectures. *Quantum Science and Technology* **5** (02 2020). <https://doi.org/10.1088/2058-9565/ab79b1>
15. Paler, A.: On the influence of initial qubit placement during nisq circuit compilation (11 2018)
16. Preskill, J.: Quantum computing in the nisq era and beyond. *Quantum* **2** (2018)
17. Shafaei, A., Saeedi, M., Pedram, M.: Optimization of quantum circuits for interaction distance in linear nearest neighbor architectures. *Proceedings - Design Automation Conference* pp. 1–6 (05 2013). <https://doi.org/10.1145/2463209.2488785>
18. Shafaei, A., Saeedi, M., Pedram, M.: Optimization of quantum circuits for interaction distance in linear nearest neighbor architectures (2013)
19. Siraichi, M.Y., dos Santos, V.F., Collange, S., Pereira, F.M.Q.: Qubit allocation (2018)
20. Sun, S., Luo, Q.: In-memory subgraph matching: An in-depth study pp. 1083–1098 (06 2020). <https://doi.org/10.1145/3318464.3380581>
21. Tannu, S., Qureshi, M.: Not all qubits are created equal: A case for variability-aware policies for nisq-era quantum computers pp. 987–999 (04 2019). <https://doi.org/10.1145/3297858.3304007>
22. Venturelli, D., do, M., Rieffel, E., Frank, J.: Temporal planning for compilation of quantum approximate optimization circuits pp. 4440–4446 (08 2017). <https://doi.org/10.24963/ijcai.2017/620>
23. Xiangzhen, Z., Li, S., Feng, Y.: Quantum circuit transformation based on simulated annealing and heuristic search. *IEEE Transactions on Computer-Aided Design of Integrated Circuits and Systems* **PP**, 1–1 (01 2020). <https://doi.org/10.1109/TCAD.2020.2969647>

24. Zhang, Y., Deng, H., Li, Q., Haoze, S., Nie, L.: Optimizing quantum programs against decoherence: Delaying qubits into quantum superposition pp. 184–191 (07 2019). <https://doi.org/10.1109/TASE.2019.000-2>
25. Zulehner, A., Paller, A., Wille, R.: Efficient mapping of quantum circuits to the ibm qx architectures. *IEEE Transactions on Computer-Aided Design of Integrated Circuits and Systems* (12 2017). <https://doi.org/10.1109/TCAD.2018.2846658>

A Experimental details of the *SWAP* gates added by the output circuits

Circuit name	qubit no.	<i>CNOT</i> no.	TST_{num} added	TST_{dep} added	optm added	wghtgr added
decod24-enable_126	6	149	28	42	60	16
4mod5-v0_19	5	16	0	0	0	0
4mod5-v0_18	5	31	2	5	4	4
mod5d2_64	5	25	5	6	8	3
4gt4-v0_72	6	113	14	10	33	14
alu-v3_35	5	18	2	4	8	2
4gt4-v0_73	6	179	27	34	76	12
alu-v3_34	5	24	2	3	7	2
3_17_13	3	17	0	0	6	0
4gt4-v0_78	6	109	12	8	48	4
4gt4-v0_79	6	105	17	17	48	3
4mod7-v1_96	5	72	16	19	27	7
mod10_171	5	108	17	20	39	9
ex2_227	7	275	48	59	121	33
mod10_176	5	78	14	14	38	8
0410184_169	5	9	2	2	49	3
4mod5-v0_20	5	10	0	0	4	0
aj-e11_165	5	69	8	8	33	7
alu-v1_28	5	18	2	4	11	2
4gt12-v0_86	6	116	28	33	48	3
4gt12-v0_87	6	112	27	32	45	2
4gt12-v0_88	6	86	5	5	25	4
alu-v1_29	5	17	4	4	11	2
ham7_104	7	149	28	34	68	12
C17_204	7	205	26	53	99	22
xor5_254	6	5	0	0	1	0
hwb4_49	5	107	14	15	38	11
rd73_140	10	104	23	26	35	20
decod24-v0_38	4	23	0	0	6	0
rd53_131	7	200	39	39	98	24
rd53_133	7	256	37	47	102	27
rd53_135	7	134	28	29	38	23
decod24-v2_43	4	22	0	0	9	0
rd53_138	8	60	14	16	23	9
rd32-v0_66	4	16	0	0	6	0
4gt13-v1_93	5	30	0	0	13	0
graycode6_47	6	5	0	0	0	0
4mod5-bdd_287	7	31	3	6	8	6
ham3_102	3	11	0	0	3	0
4gt4-v0_80	6	79	5	5	22	5
ex-1_166	3	9	0	0	3	0
mod5mils_65	5	16	0	0	6	0
0example	5	9	1	2	3	3
alu-v4_36	5	51	12	8	22	4
alu-v4_37	5	18	2	4	8	2
ex1_226	6	5	0	0	1	0
one-two-three-v0_98	5	65	11	13	32	10
one-two-three-v0_97	5	128	23	23	64	16
one-two-three-v3_101	5	32	3	4	14	3
rd32_270	5	36	3	3	6	6

Table 3. Comparison of the number of *SWAP* gates added by the output circuit on the IBM Q20

Circuit name	qubit no.	$CNOT$ no.	TST_{num} added	TST_{dep} added	optm added	wghtgr added
rd53_130	7	448	89	100	190	49
rd53_251	8	564	104	131	230	45
4mod5-v1_24	5	16	0	0	3	0
mod5adder_127	6	239	21	56	111	20
4_49_16	5	99	20	17	40	10
hwb5_53	6	598	141	168	173	59
ex3_229	6	175	10	9	50	11
4gt10-v1_81	5	66	14	15	28	6
alu-v2_32	5	72	15	17	27	7
alu-v2_31	5	198	42	54	85	13
alu-v2_30	6	223	41	45	96	20
sf_276	6	336	12	52	138	12
decod24-v1_41	5	38	4	4	14	3
sf_274	6	336	34	21	82	12
4gt4-v1_74	6	119	17	24	37	9
alu-v2_33	5	17	4	4	8	2
cnt3-5_179	16	85	6	6	35	4
4mod5-v1_22	5	11	0	0	5	0
4mod5-v1_23	5	32	5	5	4	3
mini_alu_305	10	77	10	20	28	8
alu-v0_26	5	38	7	10	13	3
alu-bdd_288	7	38	4	12	16	6
alu-v0_27	5	17	2	4	11	2
4gt13_91	5	49	7	7	10	2
4gt5_77	5	58	12	12	20	6
4gt13_92	5	30	0	0	14	0
4gt5_76	5	46	7	10	24	5
4gt5_75	5	38	5	12	16	4
4gt12-v1_89	6	100	11	21	38	4
one-two-three-v1_99	5	59	12	10	26	7
4gt13_90	5	53	7	7	13	3
ising_model_10	10	90	0	0	5	0
4gt11_84	5	9	0	0	3	0
4gt11_83	5	14	0	0	0	0
mod5d1_63	5	13	0	0	1	0
4gt11_82	5	18	1	1	1	1
decod24-v3_45	5	64	15	15	32	8
rd32-v1_68	4	16	0	0	6	0
mini_alu_167	5	126	27	27	49	11
one-two-three-v2_100	5	32	3	4	8	3
4mod7-v0_94	5	72	8	13	36	9
cm82a_208	8	283	41	69	84	33
mod8-10_178	6	152	5	20	13	7
mod8-10_177	6	196	14	33	58	13
majority_239	7	267	39	43	105	33
miller_11	3	23	0	0	9	0
decod24-bdd_294	6	32	4	4	9	4
total	551	9244	1372	1738	3481	800

Table 4. Comparison of the number of *SWAP* gates added by the output circuit on the IBM Q20

Circuit name	qubit no.	$CNOT$ no.	TST_{num} added	TST_{dep} added	optm added	wghtgr added
max46_240	10	11844	3473	4545	-	-
rd73_252	10	2319	586	761	-	-
cycle10_2_110	12	2648	919	1216	961	-
sqrt8_260	12	1314	379	492	457	-
urf4_187	11	224028	54785	60140	-	-
sqn_258	10	4459	1199	1420	-	-
f2_232	8	525	87	124	218	-
radd_250	13	1405	386	489	511	-
ham15_107	15	3858	1326	1689	-	-
sao2_257	14	16864	5346	7178	-	-
sym9_148	10	9408	1865	2432	-	-
urf5_280	9	23764	6989	8730	-	-
square_root_7	15	3089	812	2150	-	-
sys6-v0_111	10	98	23	26	38	-
hwb7_59	8	10681	2687	3551	3722	-
sym9_146	12	148	38	55	54	-
wim_266	11	427	93	120	147	-
urf2_152	8	35210	9181	11921	10577	-
urf5_159	9	71932	20258	25505	-	-
urf2_277	8	10066	2807	3798	3782	-
life_238	11	9800	2762	3576	-	-
root_255	13	7493	2128	3035	-	-
9symml_195	11	15232	4553	5986	-	-
sym10_262	12	28084	8534	11033	-	-
dc1_220	11	833	226	207	371	-
cm42a_207	14	771	182	229	294	-
rd53_311	13	124	26	48	47	-
dc2_222	15	4131	1383	1773	-	-
rd84_142	15	154	49	58	50	-
sym6_145	7	1701	317	449	750	-
co14_215	15	7840	3078	3819	-	-
cnt3-5_180	16	215	59	74	79	-
cm152a_212	12	532	103	129	168	-
sym6_316	14	123	30	39	56	-
mlp4_245	16	8232	2780	3490	-	-
hwb8_113	9	30372	10749	16489	-	-
qft_16	16	240	90	147	-	-
plus63mod4096_163	13	56329	19759	24273	-	-
urf1_149	9	80878	22551	28516	-	-
urf3_155	10	185276	50842	62903	-	-
urf3_279	10	60380	17999	23318	-	-
hwb9_119	10	90955	22946	30031	-	-
plus63mod8192_164	14	81865	28022	36207	-	-
pm1_249	14	771	182	229	294	-
sym9_193	11	15232	4382	5518	-	-
misex1_241	15	2100	480	754	600	-
urf1_278	9	26692	8010	10217	-	-
squar5_261	13	869	219	313	290	-
ground_state_estimation_10	13	154209	11671	22886	-	-
adr4_197	13	1498	516	670	-	-

Table 5. Comparison of the number of *SWAP* gates added by the output circuit on the IBM Q20

Circuit name	qubit no.	$CNOT$ no.	TST_{num} added	TST_{dep} added	optm added	wghtgr added
hwb6_56	7	2952	698	933	909	-
clip_206	14	14772	5430	6865	-	-
cm85a_209	14	4986	2088	2225	-	-
rd84_253	12	5960	1849	2333	-	-
dist_223	13	16624	5623	7431	-	-
inc_237	16	4636	1193	1667	-	-
qft_10	10	90	23	34	30	-
urf6_160	15	75180	27524	32452	-	-
con1_216	9	415	86	118	177	-

Table 6. Comparison of the number of $SWAP$ gates added by the output circuit on the IBM Q20

B Experimental details of the depths of the output circuits

Circuit name	qubit no.	$CNOT$ no.	depths no.	TST_{num} depths	TST_{dep} depths	optm depths
decod24-enable_126	6	149	190	233	275	470
4mod5-v0_19	5	16	21	16	16	21
4mod5-v0_18	5	31	40	37	46	54
mod5d2_64	5	25	32	40	43	67
4gt4-v0_72	6	113	137	155	143	297
alu-v3_35	5	18	22	24	30	60
4gt4-v0_73	6	179	227	260	281	586
alu-v3_34	5	24	30	30	33	63
3_17_13	3	17	22	17	17	52
4gt4-v0_78	6	109	137	145	133	352
4gt4-v0_79	6	105	132	156	156	345
4mod7-v1_96	5	72	94	120	129	218
mod10_171	5	108	139	159	168	335
ex2_227	7	275	355	419	452	899
mod10_176	5	78	101	120	120	274
cycle10_2_110	12	2648	3386	5405	6296	7467
0410184_169	5	9	6	15	15	253
4mod5-v0_20	5	10	12	10	10	32
sqrt8_260	12	1314	1661	2451	2790	3561
aj-e11_165	5	69	86	93	93	250
alu-v1_28	5	18	22	24	30	70
f2_232	8	525	668	786	897	1672
radd_250	13	1405	1781	2563	2872	3985
4gt12-v0_86	6	116	135	200	215	334
4gt12-v0_87	6	112	131	193	208	324
4gt12-v0_88	6	86	108	101	101	222
alu-v1_29	5	17	22	29	29	64
ham7_104	7	149	185	233	251	491
C17_204	7	205	253	283	364	688
xor5_254	6	5	5	5	5	10
hwb4_49	5	107	134	149	152	308
rd73_140	10	104	92	173	182	185
decod24-v0_38	4	23	30	23	23	61
rd53_131	7	200	261	317	317	677
rd53_133	7	256	327	367	397	777
rd53_135	7	134	159	218	221	331
sys6-v0_111	10	98	75	167	176	188
decod24-v2_43	4	22	30	22	22	75
hwb7_59	8	10681	13437	18742	21334	29601
rd53_138	8	60	56	102	108	114
rd32-v0_66	4	16	20	16	16	51
sym9_146	12	148	127	262	313	309
4gt13-v1_93	5	30	39	30	30	102
graycode6_47	6	5	5	5	5	5
wim_266	11	427	514	706	787	1180
urf2_152	8	35210	44100	62753	70973	90299
urf2_277	8	10066	11390	18487	21460	26548
4mod5-bdd_287	7	31	41	40	49	71
ham3_102	3	11	13	11	11	28
4gt4-v0_80	6	79	101	94	94	206

Table 7. Comparison of the depth of the output circuit on the IBM Q20

Circuit name	qubit no.	$CNOT$ no.	depths no.	TST_{num} depths	TST_{dep} depths	optm depths
ex-1.166	3	9	12	9	9	28
mod5mils.65	5	16	21	16	16	52
0example	5	9	6	12	15	15
alu-v4.36	5	51	66	87	75	170
alu-v4.37	5	18	22	24	30	60
ex1.226	6	5	5	5	5	10
one-two-three-v0.98	5	65	82	98	104	234
one-two-three-v0.97	5	128	163	197	197	443
one-two-three-v3.101	5	32	40	41	44	95
rd32.270	5	36	47	45	45	76
dc1.220	11	833	1041	1511	1454	2711
rd53.130	7	448	569	715	748	1417
rd53.251	8	564	712	876	957	1767
cm42a.207	14	771	940	1317	1458	2279
rd53.311	13	124	130	202	268	300
4mod5-v1.24	5	16	21	16	16	36
mod5adder.127	6	239	302	302	407	817
4.49.16	5	99	125	159	150	320
hwb5.53	6	598	758	1021	1102	1560
ex3.229	6	175	226	205	202	462
rd84.142	15	154	110	301	328	253
4gt10-v1.81	5	66	84	108	111	210
alu-v2.32	5	72	92	117	123	215
alu-v2.31	5	198	255	324	360	650
alu-v2.30	6	223	285	346	358	734
sym6.145	7	1701	2187	2652	3048	5716
sf.276	6	336	435	372	492	1096
decod24-v1.41	5	38	50	50	50	120
sf.274	6	336	436	438	399	822
4gt4-v1.74	6	119	154	170	191	329
alu-v2.33	5	17	22	29	29	59
cnt3-5.180	16	215	209	392	437	482
cm152a.212	12	532	684	841	919	1423
cnt3-5.179	16	85	61	103	103	166
sym6.316	14	123	135	213	240	378
4mod5-v1.22	5	11	12	11	11	37
4mod5-v1.23	5	32	41	47	47	55
mini_alu.305	10	77	71	107	137	187
alu-v0.26	5	38	49	59	68	108
alu-bdd.288	7	38	48	50	74	112
alu-v0.27	5	17	21	23	29	63
4gt13.91	5	49	61	70	70	108
4gt5.77	5	58	74	94	94	170
4gt13.92	5	30	38	30	30	103
4gt5.76	5	46	56	67	76	171
4gt5.75	5	38	47	53	74	127
4gt12-v1.89	6	100	130	133	163	313
one-two-three-v1.99	5	59	76	95	89	194
4gt13.90	5	53	65	74	74	124
pm1.249	14	771	940	1317	1458	2279

Table 8. Comparison of the depth of the output circuit on the IBM Q20

Circuit name	qubit no.	$CNOT$ no.	depths no.	TST_{num} depths	TST_{dep} depths	optm depths
ising_model_10	10	90	52	90	90	107
misex1_241	15	2100	2676	3540	4362	5326
4gt11_84	5	9	11	9	9	25
4gt11_83	5	14	16	14	14	16
mod5d1_63	5	13	13	13	13	17
4gt11_82	5	18	20	21	21	25
squar5_261	13	869	1051	1526	1808	2309
decod24-v3_45	5	64	84	109	109	244
rd32-v1_68	4	16	21	16	16	52
hwb6_56	7	2952	3736	5046	5751	7773
mini-alu_167	5	126	162	207	207	400
one-two-three-v2_100	5	32	40	41	44	80
4mod7-v0_94	5	72	92	96	111	270
cm82a_208	8	283	340	406	490	699
mod8-10_178	6	152	193	167	212	243
mod8-10_177	6	196	251	238	295	525
majority_239	7	267	344	384	396	839
qft_10	10	90	37	159	192	135
miller_11	3	23	29	23	23	75
decod24-bdd_294	6	32	40	44	44	86
con1_216	9	415	508	673	769	1197
total	823	83416	103023	145372	164848	224731

Table 9. Comparison of the depth of the output circuit on the IBM Q20

Circuit name	qubit no.	$CNOT$ no.	depths no.	TST_{num} depths	TST_{dep} depths	optm depths
max46_240	10	11844	14257	22263	25479	-
rd73_252	10	2319	2867	4077	4602	-
urf4_187	11	224028	264330	388383	404448	-
sqn_258	10	4459	5458	8056	8719	-
ham15_107	15	3858	4819	7836	8925	-
sao2_257	14	16864	19563	32902	38398	-
sym9_148	10	9408	12087	15003	16704	-
urf5_280	9	23764	27822	44731	49954	-
square_root_7	15	3089	3847	5525	9539	-
urf5_159	9	71932	89148	132706	148447	-
life_238	11	9800	12511	18086	20528	-
root_255	13	7493	8839	13877	16598	-
9symml_195	11	15232	19235	28891	33190	-
sym10_262	12	28084	35572	53686	61183	-
dc2_222	15	4131	5242	8280	9450	-
co14_215	15	7840	8570	17074	19297	-
mlp4_245	16	8232	10328	16572	18702	-
hwb8_113	9	30372	38717	62619	79839	-
qft_16	16	240	61	510	681	-
plus63mod4096_163	13	56329	72246	115606	129148	-
urf1_149	9	80878	99586	148531	166426	-
urf3_155	10	185276	229365	337802	373985	-
urf3_279	10	60380	70702	114377	130334	-
hwb9_119	10	90955	116199	159793	181048	-
plus63mod8192_164	14	81865	105142	165931	190486	-
sym9_193	11	15232	19235	28378	31786	-
ising_model_13	13	120	46	120	120	-
urf1_278	9	26692	30955	50722	57343	-
ising_model_16	16	150	57	150	150	-
ground_state_estimation_10	13	154209	217236	189222	222867	-
adr4_197	13	1498	1839	3046	3508	-
clip_206	14	14772	17879	31062	35367	-
cm85a_209	14	4986	6374	11250	11661	-
rd84_253	12	5960	7261	11507	12959	-
dist_223	13	16624	19694	33493	38917	-
inc_237	16	4636	5864	8215	9637	-
urf6_160	15	75180	93645	157752	172536	-

Table 10. Comparison of the depth of the output circuit on the IBM Q20